OPEN ACCESS

Communication—Capillary Effects on Metal Cation Solubility

Journal of The Electrochemical Society, 2023 **170** 111503

Communication—Capillary Effects on Metal Cation Solubility

Karl Sieradzki[z]

Ira A. Fulton School of Engineering, Arizona State University, Tempe, Arizona 85287, United States of America

The effect of capillarity on the chemical equilibrium between a dissolved metal cation and the corresponding metal oxide is determined within the framework of Gibbssian thermodynamics. We examined the equilibrium between Cr^{3+} and Cr_2O_3 and found that for 10^{-6} M Cr^{3+} in the electrolyte and a curvature of -2×10^9 m^{-1}, the equilibrium pH is -1.8. The corresponding potential-pH diagram shows that chromium passivates in strong acids. This analysis potentially resolves a long-standing issue in corrosion science.

 [DOI: 10.1149/1945-7111/ad0e48]

Manuscript submitted October 6, 2023; revised manuscript received November 15, 2023. Published November 29, 2023.

This manuscript is motivated by thermodynamic predictions of potential-pH diagrams that conclude that for many elemental metals, passivation does not occur in non-complexing strong acids.[1] For the prototypical case of Cr, Pourbaix considers the following chemical equilibria between Cr_o^{2+}/CrO and Cr_o^{3+}/Cr_2O_3.

$$Cr_o^{2+} + H_2O = CrO + 2H^+ \quad [1]$$

$$2Cr_o^{3+} + 3H_2O = Cr_2O_3 + 6H^+ \quad [2]$$

The corresponding Cr-cation solubilities in equilibrium with the respective oxides are given by.

$$\log(Cr_o^{2+}) = 10.99 - 2\,pH \quad [1']$$

$$\log(Cr_o^{3+}) = 8.39 - 3\,pH \quad [2']$$

According to these equations at a Cr_o^{3+} concentration of 10^{-6} M, elemental Cr can only passivate at a pH $\geqslant$ 4.8. While the situation for the equilibrium between Cr_o^{3+} and $Cr(OH)_3$ shows somewhat lower solubility of Cr_o^{3+}, $log(Cr_o^{3+}) = 4.60 - 3$ pH, passivation is still not predicted below a pH of 3.5.

The data Pourbaix used for the thermodynamic calculations derive from the chemical potentials of the bulk oxides or hydroxides and the source for the data was W.M. Latimer.[2] Modern DFT calculations of chemical equilibria between Cr oxide or hydroxide and Cr_o^{2+} or Cr_o^{3+} show qualitatively similar results with regard to passivation in a strong acid.[3]

Herein, we suggest that these thermodynamic calculations are subject to an important *caveat,* that the metal cation-oxide/hydroxide equilibria considered are for a planar zero-curvature surface. Importantly, capillary effects are well known to alter the equilibrium conditions as expressed by the Kelvin or Gibbs-Thomson equations. As shown in Fig. 1, we can use a simple heuristic argument to clarify the chemical physics for how capillarity can alter metal cation solubilities. Figure 1a illustrates a small section of a real surface with nanoscale roughness. A Cr_2O_3 molecule on the surface of the nanoparticle in Fig. 1b has fewer 1st, 2nd, 3rd, etc nearest neighbors than a molecule on a planar surface. Therefore, the molecules are less tightly bound, and a larger concentration of Cr^{3+} in the electrolyte is required to maintain equilibrium.[a] A Cr_2O_3 molecule on the surface of the nanohole in Fig. 1c has more 1st, 2nd, 3rd, etc. nearest neighbors than a molecule on a planar surface so the molecules are more tightly bound. The concentration or solubility of Cr^{3+} in equilibrium with the molecules on the surface of the nanohole will be less than that required for a planar surface.

Previous work, considered how curvature affects the electrochemical stability of positive curvature Pt and Cu nanoparticles.[4–6] Those analyses resulted in particle-size dependent potential-pH diagrams. In what follows, I briefly summarize the formalism connected to how curvature alters metal cation solubility by specifically considering the Cr^{3+}/Cr_2O_3 equilibrium.

Equilibrium Conditions

The surface area of solids can change in two different ways. The surface can have atoms added to or removed while maintaining a constant atom density, or mechanical elastic strains, ε_{ij}, can result in area changes that alter the atom density on the surface. The surface free energy, γ, is the work of creating new surface at fixed atom density, while the surface stress, f, is the work of creating new surface by elastic straining and changing the surface adatom density. If we take both γ and f as isotropic, these quantities are related through the Shuttleworth equation,[7]

$$f_{ij} = \gamma_P \delta_{ij} + \partial\gamma_P/\partial\varepsilon_{ij} \quad [3]$$

This relation can be simplified in a Lagrangian coordinate system.[8] The Lagrangian area, A, is connected to the physical area, A_P, by

$$A = A_P/(1 + \varepsilon_{ii}) \quad [4]$$

where the repeated index signifies the summation convention. The two ways to alter the area correspond respectively to a change in A while holding ε_{ij} constant and to a change in ε_{ij} holding A constant. In the Lagrangian system of measure,

$$f_{ij} = \partial\gamma/\partial\varepsilon_{ij} \quad [5]$$

Since, $\gamma = \gamma_P(1 + \varepsilon_{ii})$, equivalent results in the physical and Lagrangian systems are obtained. For the purposes of simplifying our presentation, Lagrangian coordinates are used in what follows.

Capillary effects in fluid/vapor systems are well known and understood. Mechanical equilibrium requires that there is a pressure difference between a spherical drop of radius, r, and the pressure of the vapor. This pressure difference between fluid and vapor, called the Laplace pressure, is $\gamma(2/r)$ where γ is the interfacial free energy of the liquid/vapor interface. A similar consideration for a finite size, single component solid immersed in a fluid is given by $f(2/r)$, where f is the interfacial stress. We note that in the case of liquids, $f = \gamma$, while for real solids this is rarely the case. This difference in the Laplace pressure for a finite size crystalline solid and a liquid means that at equilibrium there is a difference in the chemical potential, μ, of the component in the solid and fluid phase given by[5,8,9]

[z]E-mail: karl.sieradzki@asu.edu

[a]Cr_o^{3+} corresponds to the equilibrium concentration for a flat planar surface, while Cr^{3+} is that for a curved surface.

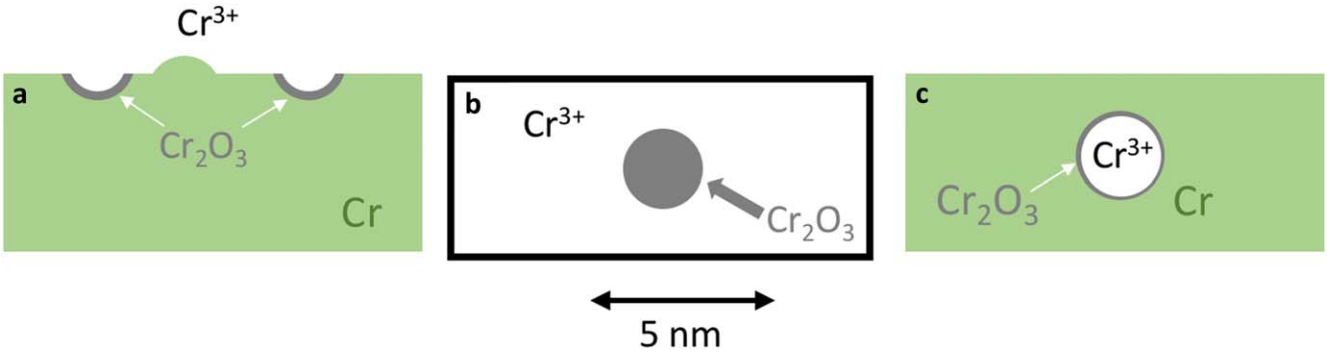

Figure 1. Cartoon illustrating the effect of curvature on the chemical equilibrium between Cr^{3+} and Cr_2O_3. (a) A small portion of a surface containing nanometer scale hemispherical holes and mounds. (b) A Cr_2O_3 spherical positive curvature nanoparticle in equilibrium with Cr cations. (c) Equilibrium of spherical negative curvature nanometer scale hole filled with Cr cations.

$$\mu_s - \mu_l = (f - \gamma)V(2/r) \quad [6]$$

where V is the molar volume of the solid. Note that for equilibrium between a planar solid surface ($r \Rightarrow \infty$) and a fluid phase, the standard equilibrium condition, $\mu_s = \mu_l$ is recovered.

In a multicomponent solid, components can take up interstitial or substitutional lattice sites. When the component of interest is in a substitutional site, equilibrium is expressed by Eq. 6. If the component takes up interstitial sites, then in the Lagrangian system, the equilibrium is defined by an equality of chemical potentials of that component in the two phases,[8]

$$\mu_s = \mu_l \quad [7]$$

The chemical equilibrium that we consider is given by, $2Cr^{3+} + 3H_2O = Cr_2O_3 + 6H^+$. Recent ab initio DFT calculations indicate that at least initially oxygen anions incorporate into sub-surface tetrahedral interstitial sites.[10,11] The chemical potential of component Cr^{3+} in the liquid phase is,

$$\mu^l_{Cr^{3+}} = \mu(Cr_0^{3+}) + RT \ln\left(\frac{Cr^{3+}}{Cr_0^{3+}}\right) \quad [8]$$

where Cr_0^{3+} is the saturation concentration of Cr^{3+} at a flat, zero curvature interface and Cr^{3+} is the saturation concentration for a surface of finite radius. The chemical potential of the solid containing component Cr^{3+} is

$$\mu^s_{Cr^{3+}} = \mu(Cr_0^{3+}) + f_{Cr_2O_3}\overline{V}_{Cr_2O_3}(2/r) \quad [9]$$

where $\overline{V}_{Cr_2O_3}$ is the partial molal volume of the oxide in the Cr lattice. Equations 8 and 9 define the chemical potentials for both the interstitial and substitutional case. For the interstitial case, application of Eq. 7 yields

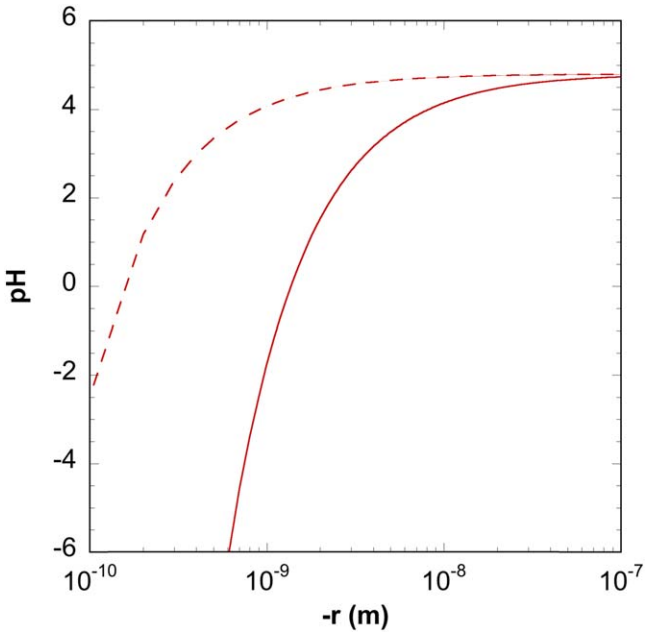

Figure 2. Cr^{3+}/Cr_2O_3 chemical equilibrium. Solid line is for the O^{2-} occupying substitutional sites and dashed line interstitial sites.

$$RT \ln\left(\frac{Cr^{3+}}{Cr_0^{3+}}\right) = f_{Cr_2O_3}\overline{V}_{Cr_2O_3}(2/r) \quad [10]$$

If O^{2-} takes up substitutional sites in the lattice, substitution of Eqs. 8 and 9 in to Eq. 6 yields,

Table I. Parameter values used in the analysis.

Parameter	Value	Method of calculation
Molar volume of Cr_2O_3: $V_{Cr_2O_3}$	2.9×10^{-5} m^3	Molar weight/density
Molar volume of Cr: V_{Cr}	7.2×10^{-6} m^3	Molar weight/density
Part. mol. vol. of Cr_2O_3: $\overline{V}_{Cr_2O_3}$	1.45×10^{-5} m^3	2 M of Cr: 1 M Cr_2O_3
Average molar volume V_o	1.81×10^{-5} m^3	$(0.5 \times V_{Cr}) + (0.5 \times V_{Cr_2O_3})$
Surface energy of Cr_2O_3: $\gamma_{Cr_2O_3}$	3.20 Jm^{-2}	14
Surface stress of Cr_2O_3: $f_{Cr_2O_3}$	0.43 Jm^{-2}	5
Surface energy of Cr: γ_{Cr}	3.5 Jm^{-2}	12, 13, 17
Surface stress of Cr: f_{Cr}	0.8 Jm^{-2}	15

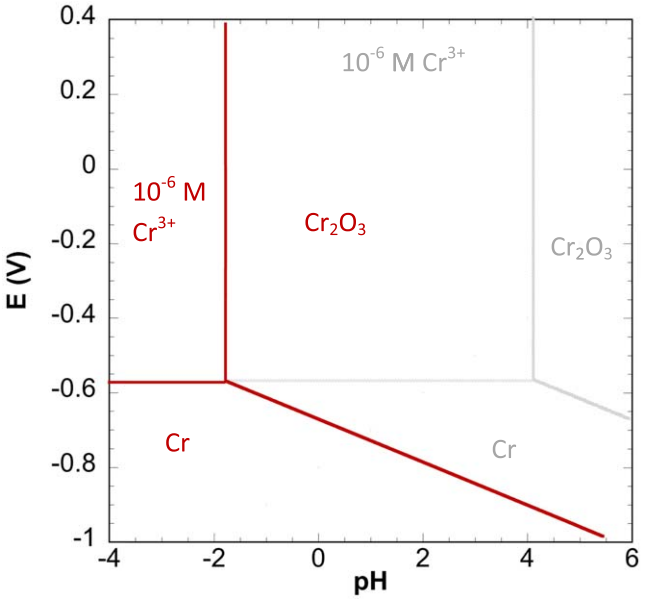

Figure 3. Chromium potential-pH diagram showing the acid region for a 2 nm diameter hemispherical hole and 10^{-6} M Cr^{3+} in the electrolyte. Solid red lines are for O^{2-} occupying substitutional sites and light gray lines for interstitial sites.

$$f_{Cr_2O_3}\bar{V}_{Cr_2O_3}(2/r) - RT\ln\left(\frac{Cr^{3+}}{Cr_0^{3+}}\right) = (f_{Cr_2O_3} - \gamma_{Cr_2O_3})V_o(2/r),$$

and rearranging,

$$RT\ln\left(\frac{Cr^{3+}}{Cr_0^{3+}}\right) = [\gamma_{Cr_2O_3}V_o + f_{Cr_2O_3}(\bar{V}_{Cr_2O_3} - V_o)](2/r) \qquad [11]$$

Here V_o is the average molar volume of the Cr-Cr_2O_3 alloy. As oxygen anions take up substitutional lattice sites, the surface energy changes with the strain. This elastic strain results from the difference in the quantity $(\bar{V}_{Cr_2O_3} - V_o)$. Since 2 moles of Cr are required to form 1 mole of Cr_2O_3, we adopt a value of the partial molal volume of Cr_2O_3 in the Cr lattice equal to half the Cr_2O_3 molar volume. There are several references for the surface energy of Cr_2O_3[14–16] and no data, that we are aware of, for the surface stress. Nevertheless, we will proceed by estimating a value of surface stress based on the ratio of the surface stress of elemental Pt and its oxide.[5]

Substitution of Eq. 2′ for Cr_0^{3+}, $T = 298$ K, and the parameter values from Table I into Eqs. 10 and 11 yield Eq. 10′) and 11′. The results for the equilibrium pH as a function of the hole radius are shown in Fig. 2 for 10^{-6} M Cr^{3+} in the electrolyte.

$$pH = 4.8 + 7.28 \times 10^{-10}(1/r) \qquad [10']$$

$$pH = 4.8 + 6.57 \times 10^{-9}(1/r) \qquad [11']$$

In these equations, r values with the appropriate sign need to be used. Equation 10′ (interstitial sites) indicates that surface roughness containing negative curvatures, κ, (=−2/r), of -1.32×10^{10} m^{-1} or smaller are required to observe passivation of Cr at pH = 0 for 10^{-6} M Cr^{3+} in the acid. For the same electrolyte chemistry Eq. 13′ (substitutional sites) predicts values of -1.46×10^{9} m^{-1}.

Surface roughness features below about 10 nm in size cannot be removed from the surface of a real metal by any process that we are familiar with. Additionally, the process of removal of an air-formed film by electrochemical reduction will likely result in additional roughness.[18] Alloys such as Fe-Cr, Ni-Cr and 300 series stainless steels undergo selective dissolution prior to passivation, which also results in nanoscale surface roughness.[19–21]

Cr Potential-pH Diagram

In order to evaluate how curvature affects the conventional Pourbaix diagram for Cr we develop a diagram based on the data in Table I for interstitial and substitutional occupation. We only consider the case of Cr^{3+}/Cr_2O_3 equilibrium, since there is no data available for the surface energy of CrO. In addition to 10′ and 11′, we require the curvature effect for the Cr equilibrium reaction, $Cr^{3+} + 3\,e^- = Cr$ and that for the equilibrium of Cr and Cr_2O_3, $Cr_2O_3 + 6H^+ + 6e^- = 2Cr + 3H_2O$. The chemical potential of Cr in the nanoscale spherical particle or hemispherical hole is

$$\mu_{Cr}^{s} = \mu(Cr_0^{3+}) + f_{Cr}V_{Cr}(2/r) \qquad [12]$$

The chemical potential of Cr^{3+} in the liquid is given by Eq. 8. Applying the equilibrium condition, Eq. 6,

$$RT\ln\left(\frac{Cr^{3+}}{Cr_0^{3+}}\right) = \gamma_{Cr}V_{Cr}(2/r) \qquad [13]$$

Since $\Delta G = -nFE$,

$$E = E^0_{Cr^{3+}} - \frac{\gamma_{Cr}V_{Cr}}{3F}(2/r), \qquad [14]$$

where, $E^0_{Cr^{3+}}$ is the standard potential for the reaction equal to −0.744 V (SHE). For a 1 nm radius semi-circular hole in the surface, the curvature is $(-2/r) = -2 \times 10^9$ m^{-1}. Inserting the parameter values from the data set in Table I for 10^{-6} M Cr^{3+}, for the substitutional case we obtain,

$$\mathrm{E} = -0.570\ \mathrm{V} \qquad [14']$$

$$\mathrm{pH} = -1.78 \qquad [11a']$$

$$E = -0.674 - 0.059\ \mathrm{pH} \qquad [15]$$

The corresponding equations for the interstitial case are,

$$\mathrm{E} = -0.570\ \mathrm{V} \qquad [14a']$$

$$\mathrm{pH} = 4.1 \qquad [10a']$$

$$E = -0.330 - 0.059\ \mathrm{pH} \qquad [16]$$

As shown in Fig. 3, these equations are used to construct the acid region of the E-pH diagram for a surface containing 2 nm diameter hemispherical holes. The interstitial case, lowers the 10^{-6} M Cr^{3+}/Cr_2O_3 chemical equilibrium by only 0.8 pH units to 4.0 as a result of the small value of $f_{Cr_2O_3}$ that we adopted.

Conclusions

The main aim of this analysis is to demonstrate how capillarity can significantly alter the potential and pH conditions for passivation. The major unknowns in the analysis are $f_{Cr_2O_3}$, $\bar{V}_{Cr_2O_3}$ and V_o. Equations 10′ and 11′ depend on the relative values of these unknown parameters. For example, for large enough values of V_o and/or $f_{Cr_2O_3}$, the pH could shift to positive values. On the other hand, if $f_{Cr_2O_3}$ and $\bar{V}$ were larger, the pH would decrease considerably for the interstitial case. We used a value of 0.43 Jm^{-2} for $f_{Cr_2O_3}$ but a larger value would greatly alter Eq. 10′ and our passivation prediction for the case of O^{2-} interstitial site occupation. Since the value of the oxide surface stress makes a smaller contribution to Eq. 11′, the E-pH diagram would not significantly change in the case of substitutional site occupation. In principle,

excellent values of these parameters could be obtained by ab initio DFT approaches. The occurrence of nanoscale regions of positive and negative curvature on a well-prepared surface can be examined by scanning probe techniques such as atomic force or scanning tunneling microscopy. For example, one could first examine the statistics of surface roughness on air-formed films and then compare these results to those obtained on surfaces that are reduced in electrolyte and passivated at an appropriate potential. Finally, while this analysis considers only isotropic surface free energies and surface stresses, anisotropic effects could be incorporated in a more detailed analysis that will have to await the first principles-based calculations discussed above.

Acknowledgments

K.S. thanks James Rondenelli, Ian McCue and Lauren Walters for stimulating discussions, and Qingguo Bai and Roger Newman for critically reading an early version of the manuscript. This work was supported by the National Science Foundation under award DMR-2208848 and the Office of Naval Research under award number N00014–20–1–2368.

ORCID

Karl Sieradzki https://orcid.org/0000-0002-4789-3956

References

1. M. Pourbaix, *Atlas of Electrochemical Equilibria in Aqueous Solutions*, (National Association of Corrosion Engineers (NACE) Houston, Texas, USA) (1974).
2. W. M. Latimer, *The Oxidation States of the Elements and their Potentials in Aqueous Solutions* (Prentice Hall, New York, New York) (1938).
3. L. F. Huang and J. M. Rondinelli, "Reliable electrochemical phase diagrams of magnetic transition metals and related compounds from high-throughput *ab initio* calculations." *npj Mater. Degrad.*, **3**, 26 (2019).
4. L. Tang, B. Han, K. Persson, C. Friesen, T. He, K. Sieradzki1, and G. Ceder, "Electrochemical Stability of nm-Scale Pt Particles in Acidic Environments." *J. Am. Chem. Soc.*, **132**, 596 (2010).
5. L. Tang, X. Li, R. C. Cammarata, C. Friesen, and K. Sieradzki, "Electrochemical Stability of Elemental Metal Nanoparticles." *J. Am. Chem. Soc.*, **132**, 11722 (2010).
6. C. D. Taylor, M. Neurock, and J. R. Scully, "First-Principles Investigation of the Fundamental Corrosion Properties of a Model Cu_{38} Nanoparticle and the (111), (113) Surfaces." *J. Electrochem. Soc.*, **155**, C407 (2008).
7. R. Shuttleworth, "The surface tension of solids." *Proc. Phys. Soc., A*, **63**, 444 (1950).
8. J. W. Cahn, "Surface stress and the chemical equilibrium of small crystals—the case of the isotropic surface." *Acta Metall.*, **28**, 1333 (1980).
9. R. C. Cammarata, "Surface and interface stress effects in thin films." *Prog. Surf. Sci.*, **46**, 1 (1994).
10. M. Todorova, W. X. Li, M. V. Ganduglia-Pirovano, C. Stampfl, K. Reuter, and M. Scheffler, "Role of subsurface oxygen in oxide formation at transition metal surfaces." *Phys. Rev. Lett.*, **89**, 096103 (2002).
11. C. Stampfl, A. Soon, S. Piccinin, H. Shi, and H. Zhang, "Bridging the temperature and pressure gaps: close-packed transition metal surfaces in an oxygen environment." *J. Phys.: Condens. Matter*, **20**, 184021 (2008).
12. L. Vitos, A. V. Ruban, H. L. Skriver, and J. Kollar, "The Surface Energy of Metals." *Surf. Sci.*, **411**, 186 (1998).
13. R. Tran, Z. Xu, B. Radhakrishnan, D. Winston, W. Sun, K. A. Persson, and S. Ong, "Surface Energy of Elemental Metals." *Sci. Data*, **3**, 160080 (2016).
14. A. Rohrbach, J. Hafner, and G. Kresse, "*Ab initio* study of the (0001) surfaces of hematite and chromia: Influence of strong electronic correlations." *Phys. Rev. B*, **70**, 125426 (2004), N.J.
15. N. J. Mosey and E. A. Carter, "*Ab initio* LDA+U prediction of the tensile properties of chromia across multiple length scales." *J. Mech. Phys. Solids*, **57**, 287 (2009).
16. M. P. J. Punkkinen, K. Kokko1, H. Levämäki, M. Ropo, S. Lu, L. Delczeg, H. L. Zhang, E. K. Delczeg-Czirjak, B. Johansson, and L. Vitos, "Adhesion of the iron–chromium oxide interface from first-principles theory." *J. Phys. Condens. Matter*, **25**, 495501 (2013).
17. J.-Y. Lee et al., "The surface energy and stress of metals." *Surf. Sci.*, **674**, 51 (2018).
18. C. M. Vitus and A. J. Davenport, "*In situ* scanning tunneling microscopy studies of the formation and reduction of a gold oxide monolayer on Au(111)." *J. Electrochem. Soc.*, **141**, 1291 (1994).
19. D. Hamm, K. Ogle, C.-O. Olsson, S. Weber, and D. Landolt, "Passivation of Fe–Cr alloys studied with ICP-AES and EQCM." *Corros. Sci.*, **44**, 1443 (2002).
20. J. E. Castle and J. H. Qiu, "A Co-ordinated study of the passivation of alloy steels by plasma source mass spectrometry and x-ray photoelectron spectroscopy-1 characterization of the passive film." *Corros. Sci.*, **29**, 591 (1989).
21. Y. Xie et al., "A percolation theory for designing corrosion-resistant alloys." *Nat. Mater.*, **20**, 789 (2021).